Mid-wave infrared metasurface microlensed focal plane array for optical crosstalk suppression

Onur Akın[1] and Hilmi Volkan Demir[1,2,*]

[1] *Department of Electrical and Electronics Engineering, Department of Physics, UNAM – Institute of Materials Science and Nanotechnology, Bilkent University, 06800, Ankara, Turkey*

[2] *LUMINIOUS! Center of Excellence for Semiconductor Lighting and Display, School of Electrical and Electronic Engineering, and School of Physical and Mathematical Sciences, Nanynang Technological University, Nanyang Avenue, Singapore 639798, Singapore*

[*] *volkan@stanfordalumni.org*

Abstract: Spatial crosstalk is one of the fundamental drawbacks of diminishing pixel size in mid-wave infrared focal plane arrays (IR-FPAs). We proposed an IR-FPA using the concept of optical phase discontinuities for substantial optical crosstalk suppression. This IR-FPA consists of asymmetrically tailored V-shaped optical antennas. Full-wave simulations confirmed major improvements in narrowing the intensity distribution of incident light beam by over 30-folds and concentrating these distributions in the central pixel of IR-FPA by achieving optical crosstalks of <1%.

©2015 Optical Society of America

OCIS codes: (160.3918) Metamaterials; (220.3630) Lenses; (250.5403) Plasmonics.

References and links

1. Y. Li, Z.-H. Ye, W.-D. Hu, W. Lei, Y.-L. Gao, K. He, H. Hua, P. Zhang, Y.-Y. Chen, C. Lin, X.-N. Hu, R.-J. Ding, and L. He, "Numerical simulation of refractive-microlense HgCdTe infrared focal plane arrays operating in optical systems," J. Electron. Mater. **43**(8), 2879–2887 (2014).
2. J. Bai, W. Hu, N. Guo, W. Lei, Y. Lv, X. Zhang, J. Si, X. Chen, and W. Lu, "Performance optimization of InSb infrared focal-plane arrays with diffractive microlenses," J. Electron. Mater. **43**(8), 2795–2801 (2014).
3. N. Yu, P. Genevet, M. A. Kats, F. Aieta, J.-P. Tetienne, F. Capasso, and Z. Gaburro, "Light propagation with phase discontinuities: generalized laws of reflection and refraction," Science **334**(6054), 333–337 (2011).
4. M. Kang, T. Feng, H. T. Wang, and J. Li, "Wave front engineering from an array of thin aperture antennas," Opt. Express **20**(14), 15882–15890 (2012).
5. A. V. Kildishev, A. Boltasseva, and V. M. Shalaev, "Planar photonics with metasurfaces," Science **339**(6125), 1232009 (2013).
6. N. Yu and F. Capasso, "Flat optics with designer metasurfaces," Nat. Mater. **13**(2), 139–150 (2014).
7. X. Ni, N. K. Emani, A. V. Kildishev, A. Boltasseva, and V. M. Shalaev, "Broadband light bending with plasmonic nanoantennas," Science **335**(6067), 427 (2012).
8. N. Yu, F. Aieta, P. Genevet, M. A. Kats, Z. Gaburro, and F. Capasso, "A broadband, background-free quarter-wave plate based on plasmonic metasurfaces," Nano Lett. **12**(12), 6328–6333 (2012).
9. X. Yin, Z. Ye, J. Rho, Y. Wang, and X. Zhang, "Photonic spin Hall effect at metasurfaces," Science **339**(6126), 1405–1407 (2013).
10. N. Shitrit, S. Maayani, D. Veksler, V. Kleiner, and E. Hasman, "Rashba-type plasmonic metasurface," Opt. Lett. **38**(21), 4358–4361 (2013).
11. S. Sun, Q. He, S. Xiao, Q. Xu, X. Li, and L. Zhou, "Gradient-index meta-surfaces as a bridge linking propagating waves and surface waves," Nat. Mater. **11**(5), 426–431 (2012).
12. S. Sun, K. Y. Yang, C. M. Wang, T. K. Juan, W. T. Chen, C. Y. Liao, Q. He, S. Xiao, W. T. Kung, G. Y. Guo, L. Zhou, and D. P. Tsai, "High-efficiency broadband anomalous reflection by gradient meta-surfaces," Nano Lett. **12**(12), 6223–6229 (2012).
13. D. Lin, P. Fan, E. Hasman, and M. L. Brongersma, "Dielectric gradient metasurface optical elements," Science **345**(6194), 298–302 (2014).
14. F. Aieta, P. Genevet, N. Yu, M. A. Kats, Z. Gaburro, and F. Capasso, "Out-of-plane reflection and refraction of light by anisotropic optical antenna metasurfaces with phase discontinuities," Nano Lett. **12**(3), 1702–1706 (2012).
15. P. Genevet, N. Yu, F. Aieta, J. Lin, M. A. Kats, R. Blanchard, M. O. Scully, Z. Gaburro, and F. Capasso, "Ultra-thin plasmonic optical vortex plate based on phase discontinuities," Appl. Phys. Lett. **100**(1), 013101 (2012).

#246090 Received 17 Jul 2015; revised 27 Aug 2015; accepted 30 Aug 2015; published 5 Oct 2015
© 2015 OSA

16. Y. Zhao and A. Alu, "Manipulating light polarization with ultrathin plasmonic metasurfaces," Phys. Rev. B **84**(20), 205428 (2011).
17. J. Lin, P. Genevet, M. A. Kats, N. Antoniou, and F. Capasso, "Nanostructured holograms for broadband manipulation of vector beams," Nano Lett. **13**(9), 4269–4274 (2013).
18. W. T. Chen, K. Y. Yang, C. M. Wang, Y. W. Huang, G. Sun, I. D. Chiang, C. Y. Liao, W. L. Hsu, H. T. Lin, S. Sun, L. Zhou, A. Q. Liu, and D. P. Tsai, "High-efficiency broadband meta-hologram with polarization-controlled dual images," Nano Lett. **14**(1), 225–230 (2014).
19. X. Ni, A. V. Kildishev, and V. M. Shalaev, "Metasurface holograms for visible light," Nat. Commun. **4**, 2807 (2013).
20. M. A. Kats, P. Genevet, G. Aoust, N. Yu, R. Blanchard, F. Aieta, Z. Gaburro, and F. Capasso, "Giant birefringence in optical antenna arrays with widely tailorable optical anisotropy," Proc. Natl. Acad. Sci. U.S.A. **109**(31), 12364–12368 (2012).
21. A. Shaltout, V. Shalaev, and A. Kildishev, "Homogenization of bi-anisotropic metasurfaces," Opt. Express **21**(19), 21941–21950 (2013).
22. M. Farmahini-Farahani, J. Cheng, and H. Mosallaei, "Metasurfaces nanoantennas for light processing," J. Opt. Soc. Am. B **30**(9), 2365–2370 (2013).
23. F. Aieta, P. Genevet, M. A. Kats, N. Yu, R. Blanchard, Z. Gaburro, and F. Capasso, "Aberration-free ultrathin flat lenses and axicons at telecom wavelengths based on plasmonic metasurfaces," Nano Lett. **12**(9), 4932–4936 (2012).
24. X. Ni, S. Ishii, A. V. Kildishev, and V. M. Shalaev, "Ultra-thin, planar, Babinet-inverted plasmonic metalenses," Light Sci. Appl. **2**(4), e72 (2013).
25. F. Aieta, P. Genevet, M. Kats, and F. Capasso, "Aberrations of flat lenses and aplanatic metasurfaces," Opt. Express **21**(25), 31530–31539 (2013).
26. F. Aieta, M. A. Kats, P. Genevet, and F. Capasso, "Multiwavelength achromatic metasurfaces by dispersive phase compensation," Science **347**(6228), 1342–1345 (2015).
27. R. Blanchard, G. Aoust, P. Genevet, N. Yu, M. A. Kats, Z. Gaburro, and F. Capasso, "Modeling nanoscale V-shaped antennas for the design of optical phased arrays," Phys. Rev. B **85**(15), 155457 (2012).
28. E. D. Palik, *Handbook of Optical Constants of Solids* (Academic, 1991).

1. Introduction

Infrared (IR) focal plane arrays (FPAs) find important use in both civil and defense applications. Especially, mid-wave (3-5 μm band) IR-FPAs are being continuously developed and commercialized. One of the most critical parameters of these devices is the pixel pitch size. Small pixel size is essential to making compact products with high spatial resolution. Unfortunately, the problem is that, as the pixel pitch is reduced, spatial crosstalk between adjacent pixels increases tremendously as a fundamental trade-off.

Integration of microlens arrays with mid-wave IR-FPAs and mesa isolation are two different strategies used for compensating the drawbacks of decreasing pixel pitch size. Mesa isolation method is implemented by physically separating the pixels and, during this process, etching can unrecoverably damage several pixels. On the other hand, integration of microlens arrays methodology relies on controlling and managing the incident light energy flow towards each pixel without physically modifying the pixel array itself. Recently, spherically refractive microlens array integration with mid-wave HgCdTe IR-FPAs has been studied numerically and the effects of microlens radius and relative aperture on crosstalk suppression have been reported [1]. However, suppressing crosstalk by squeezing the size of the Airy disk with refractive microlenses does not solve the problem due to the emergence of strong first-order diffraction spots approximately at the centers of the adjacent pixels. Another study regarding the integration of diffractive microlens array with mid-wave InSb IRFPAs investigated the performance of a diffractive microlens system with respect to the refractive microlens system [2]. However, pixels of the InSb IR-FPA were also mesa-isolated in this study and thus the performance improvement caused by this system was due to the combined effect of both methodologies.

More recently, metasurfaces, the two-dimensional counterparts of metamaterials, have been increasingly explored [3–25]. The primary reason for this growing interest is that the metasurfaces allow for controlling the amplitude, phase and polarization state of light and controlling these attributes has opened the door for wavefront shaping, light beam designing and light direction control on a subwavelength scale [3–6]. Conceptually, abrupt phase, amplitude and/or polarization changes over the scale of the wavelength are introduced on the metasurface as light traverses it [7,8]. New phenomena including anomalous reflection,

#246090 Received 17 Jul 2015; revised 27 Aug 2015; accepted 30 Aug 2015; published 5 Oct 2015
© 2015 OSA

anomalous refraction, strong photonic spin-Hall effect and plasmonic Rashba effect have been observed following the realization of metasurfaces and these observations have led to the generalization of the laws of reflection and refraction [3,9,10]. Alternative approaches based on either reflective array metasurfaces or dielectric unit elements have also been studied for dealing with the efficiency problems confronted in several of the initial metasurface designs and both high energy conversion of propagating waves into surface waves and high efficiency anomalous reflection phenomena have been achieved [11–13]. Moreover, metasurfaces have been implemented for enabling out-of-plane refraction, generating optical vortices with a variety of topological charges, manipulating light polarization state in a controllable manner and generating holograms [14–19]. Birefringent arrays and bianisotropy have also been observed within the realm of metasurfaces [20,21].

Focusing light has also been investigated in the context of metasurfaces [22–26]. Aberration-free ultrathin flat lenses have been designed, fabricated and characterized for the operating wavelength of 1.55 μm. Additionally, focusing of visible light has been demonstrated with a similar design approach but using a different realization method [23,24]. Aberration problems of lenses including off-axis aberration, which was confronted as a drawback of flat metalenses, have also been overcome following the design of aplanatic metasurfaces [25]. Moreover, achromatic metalens designs have also been investigated for focusing light at three different wavelengths on the same focal plane [26]. However, to date focal plane arrays have not been studied using metasurfaces and optical crosstalk problem has not been addressed in such metalens arrays.

In this study, different than the previous studies, we present for the first time a metasurface-based microlensed focal plane array that relies on asymmetric optical antennas [see Fig. 1 for conceptual architecture] and quantitatively analyzed its resulting light concentrating capability, which is useful for optical crosstalk suppression in mid-wave IR-FPAs. The proposed planar metasurface is based on a two-dimensional array of asymmetrically tailored optical antennas having space-variant phase shift response and subwavelength separation. Space-variant phase shift response was realized by tuning the resonance of the optical antennas via geometrical design instead of intrinsic material properties. The first part of this study involves the design of these optical antennas followed by the analysis of their scattering characteristics with finite-difference time domain (FDTD) simulations. The second part of the study involves the design of metasurfaces for implementing microlens arrays using a specific antenna set based on the analysis carried out in the first part. Here, we demonstrated the tight light concentrating enabled by the proposed designs, reaching over 30-fold narrowing with respect to a system without microlenses. Also, we compared them with refractive microlens arrays in terms of optical crosstalk reduction, resulting in <1% optical crosstalk here. Finally, we highlighted the optimal design for implementing microlens arrays that enable strong optical crosstalk suppression and outperform refractive microlens arrays by eliminating strong first order diffraction spots observed at the center of the adjacent pixels of refractive microlens IR-FPAs.

#246090 Received 17 Jul 2015; revised 27 Aug 2015; accepted 30 Aug 2015; published 5 Oct 2015
© 2015 OSA

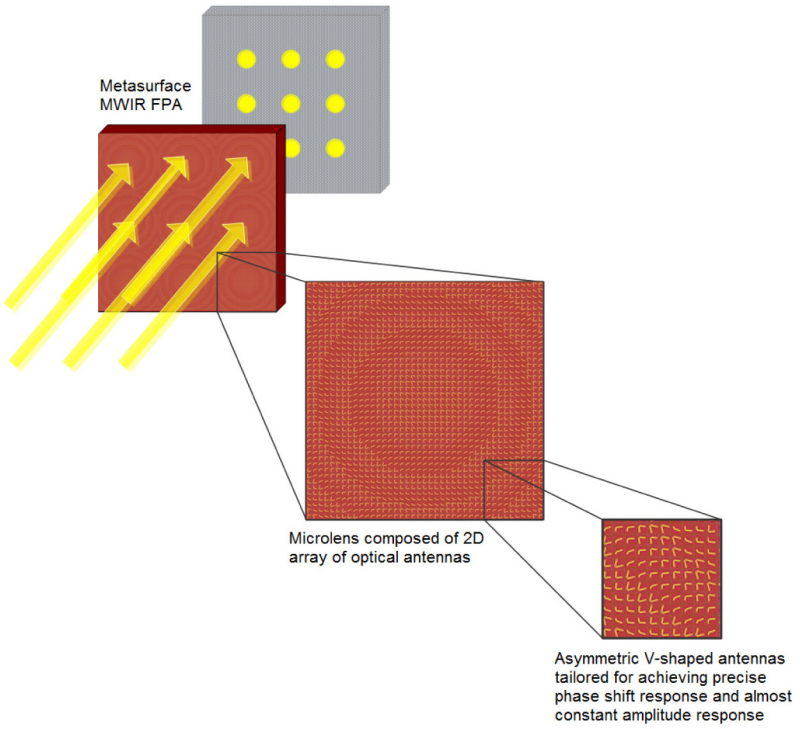

Fig. 1. Schematic representing the geometry of our proposed metasurface-based microlensed focal plane array (FPA) design. Here optical antennas are the building blocks of these microlenses in the FPA and each antenna is comprised of a pair of nanorods with space variant lengths connected head to head with space-variant angles.

2. Optical antennas as the building blocks of metasurface microlens

Building blocks of our metasurface-based microlenses are asymmetrically-tailored, V-shaped optical antennas comprised of two end-connected gold nanorods placed on a silicon substrate. Exemplary schematics showing the geometry of selected optical antennas are shown in Fig. 1. Connection angle and length of each nanorod are tuned separately for covering the full 0-to-2π phase shift response, which is necessary for designing a microlens, while the amplitude response is intended to be held almost constant for maximizing the constructive interference of the scattered fields. A set of 8 antennas are used in covering the whole phase shift range; hence, an incremental phase shift response of π/4 exists between subsequent antennas of the microlens array in the set.

Specific geometries of the optical antennas were designed by simulating every single antenna individually. Full-wave simulations were performed using Lumerical Solutions FDTD. For simulating a realistic geometry that can be easily fabricated, we designed structures similar to the V-shaped antennas studied in a previous metasurface study [27]. Cross-section of our nanorods is a square with a 100 nm width and a 100 nm thickness. For optical constants determining the optical properties of the antennas, the values found in Palik were fit to a multicoefficient model [28]. The optical antennas were also placed on the central area of a silicon substrate after observing similar results from simulations with a germanium substrate. However, we should mention that high refractive index substrate such as silicon and germanium should be used for obtaining smaller building blocks that increase the continuity of the imparted phase profile. The substrate fills half of the total simulation area, which spans 0.75 μm × 0.75 μm × 5 μm and matched by perfectly matched layers (PML) at the boundaries and the other half of the simulation area is filled by air. Meshing of the

#246090 Received 17 Jul 2015; revised 27 Aug 2015; accepted 30 Aug 2015; published 5 Oct 2015
© 2015 OSA

simulation area was carried out using a fixed mesh size of 10 nm along the lateral directions (which spans the silicon-air interface) while graded meshing was used along the normal direction to the interface. Total-field scattered-field (TFSF) planewave source that has a wavevector direction normal to the air-silicon interface and polarization direction tangential to the interface was used to illuminate the antenna from the substrate side and spans 0.7 μm × 0.7 μm × 3.5 μm. A near-field monitor was placed parallel to the interface at a distance of 1.9 μm from the interface. Then, far-field transform function called *farfieldexact* was used to obtain the amplitude and phase of the scattered field that is cross-polarized with respect to the TFSF source.

A set of 8 antennas were designed after an iterative simulation process. Length of one nanorod was varied from 300 to 600 nm while length of the other nanorod was varied from 100 to 600 nm. Connection angle of the nanorods was also varied from 50° to 150° but only specific angles, which allow for keeping the antenna inside a 750 nm × 750 nm square, were selected. The phase shift responses and scattering amplitudes of the selected antennas, which cover full 0-to-2π phase shift response with an incremental phase shift response of π/4 and have almost constant scattering amplitude, are given in Figs. 2(a) and 2(b).

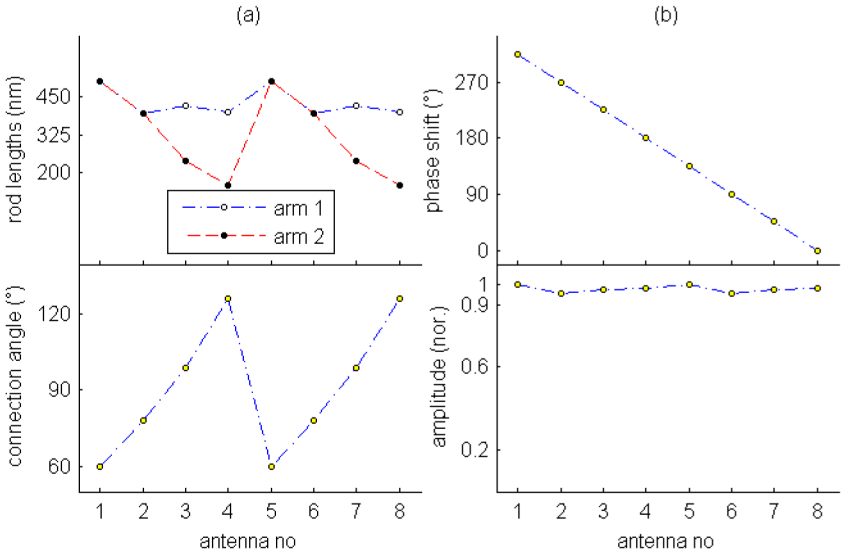

Fig. 2. (a) Rod lengths and connection angles of the individual optical antennas used to realize metalenses. (b) Phase shift responses and normalized scattering amplitudes of the individual optical antennas used to realize metalenses (Full 0-to-2π phase shift response is covered with a set of 8 antennas while amplitude response is almost held constant.)

3. Focal plane array of metasurface microlens

Focal plane array design comprises of the matrix of microlenses repeated as a unit cell in two dimensions. The main function of the microlens is to narrow the spot size of the incoming light beam captured by the cross-section of the microlens. This functionality can be realized with a metasurface having hyperboloidally varying phase shift response. Mathematical formulation of this response is given by Eq. (1) for a cylindrically symmetric structure as follows

$$\phi = \frac{2\pi}{\lambda}\left(\sqrt{r^2 + f^2} - f\right). \tag{1}$$

#246090 Received 17 Jul 2015; revised 27 Aug 2015; accepted 30 Aug 2015; published 5 Oct 2015
© 2015 OSA

where f is the focal length and r is the distance to the metasurface center while λ is the central design wavelength, here selected to be 4.3 μm (as a mid-wave IR wavelength in the band of 3-5 μm) in this study.

However, practical realization of this function with an array of antennas, each having an incremental phase shift, requires discretization of the continuous profile. This discretization process was implemented by mapping continuously changing portions of the continuous profile into constant-phase shift regions. For instance, 0-to-π/4 phase shift portion was mapped to the 0 phase shift while the π/4-to-π/2 phase shift portion was mapped to the π/4 phase shift so that only a single type of antennas (antenna no. 4) were placed in the 0 phase shift regions while another type of antennas (antenna no. 3) were placed in the π/4 phase shift region. Both the continuous phase profile and its discretization are presented in Fig. 3 for the central unit cells of the designed microlens arrays. A single unit cell of a designed microlens array has a fixed width of 30 μm, which is a commercially available mid-wave IR-FPA pixel pitch size, and contains 40 nano-antennas placed on a square silicon substrate of 750 nm side length. In determining this side length, resonance condition of the antennas was considered. This resonance condition is given by Eq. (2) where λ_0 is the free space wavelength and n_{eff} is the effective refractive index of the medium while l is the length of the antenna [27]. Using 4.3 μm as the wavelength and 2.6 as the effective refractive index resulted in l = 826 nm. Although a single wavelength was used as a starting point, the design was later checked for the entire mid-wave IR, confirming its operation across the entire band, as expected because metasurface-based metallic antennas exhibit broadband response [7, 8]. For placing antennas having comparable total lengths to this resonance length (hence a large phase shift coverage) and picking a length that is an integral divisor of 30 μm, 750 nm was determined as the side length. It is worth noting that, using this side length, neighboring V-antenna units remain uncoupled as no noticeable coupling effect between adjacent ones that change their scattering response was observed.

$$l = \frac{\lambda_0}{2n_{eff}}. \tag{2}$$

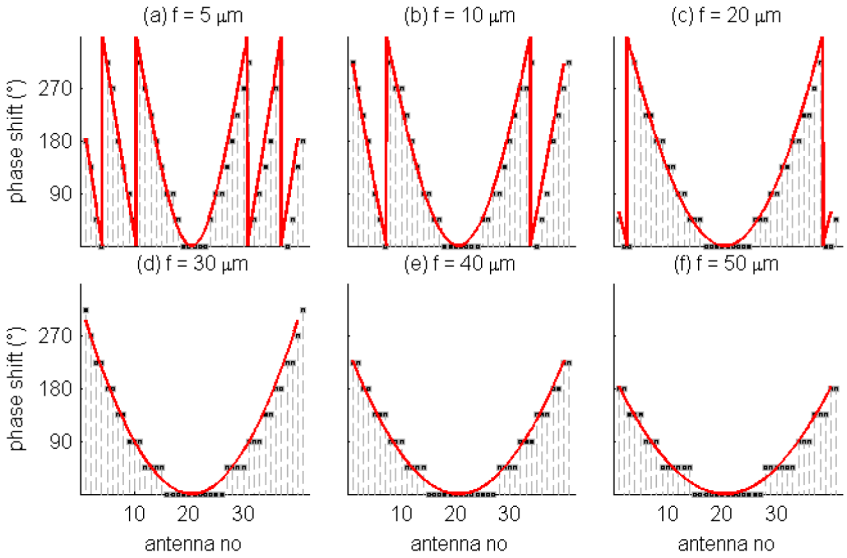

Fig. 3. (a)-(f) Phase shift responses of the antennas in the designed microlenses with focal lengths of 5, 10, 20, 30, 40 and 50 μm, represented with black squared markers, respectively. Corresponding continuous phase shift responses realized by these microlenses are also shown with red curves.

#246090 Received 17 Jul 2015; revised 27 Aug 2015; accepted 30 Aug 2015; published 5 Oct 2015
© 2015 OSA

Full-wave simulations of the designed microlens arrays were also performed using Lumerical Solutions FDTD. However, periodic boundary conditions were used instead of PML along the directions tangential to the air-silicon interface and a planewave source was used instead of the TFSF source. In order for the numerical solution to be tractable in a reasonable amount of time, we modeled cylindrical microlenses instead of spherical ones by utilizing the symmetry of the structure. Near-field distributions were recorded with a monitor placed on top of the microlens array structure (at a distance of 1.9 μm from the interface). The same far-field transformation function was used to obtain the intensity distributions (as a function of distance from the microlens array) of the cross-polarized field with respect to the source polarization. These recorded intensity distributions are given in Fig. 4 for 6 different microlens array structures corresponding to the focal length varied realizations of the hyperboloidally varying phase shift response. In these simulations, only the central unit cell of the microlens array was illuminated for analyzing the concentration of the focused light, which in the ideal case, should only be present in the central IR-FPA pixel that spans 30 μm width in the focal plane.

Optical crosstalk is characterized by point-spread function (PSF) [1]. For making a quantitive optical crosstalk analysis of the proposed designs, we integrated the corresponding areas under the PSF curve for the central pixel and its nearest neighbor pixel of the IR-FPA, respectively. For comparing the optical crosstalk performance with a system that does not include microlenses and a system that is composed of refractive microlens arrays, an intermediate $F_{\#}$ of 1.8 was chosen (which is the same as the one used in a previous microlens study [1]). After integrating the corresponding areas in the reference study, it was found that 95.7% and 94.9% of the total energy were focused to the central pixel for the system without a microlens and the refractive microlens system, respectively. However, 2.15% and 2.55% of the energy were focused to each one of the nearest neighbor pixels, respectively. Dividing these ratios resulted in 2.2% and 2.6% optical crosstalk's, respectively. This result (optical crosstalk of microlens system being higher than the reference system without microlenses) was rather surprising and explained as the consequence of the emergence of the strong first order diffraction spots at the center of the adjacent pixels, a fundamental drawback of the refractive microlens array systems. However, this drawback is completely overcome in metasurface based designs. Over 96% of the incident energy is focused in the central pixel in all of the designs with the focal length parameters of 10, 20, 30, 40 and 50 μm, with 98.4% being the highest value in the case of 10 μm focal length structure. This improvement is a direct result of the inherent non-diffractive characteristics of metasurfaces. However, we should also note that asymmetric metallic V-shaped antennas only focus cross-polarized light and, as a result, the efficiency of microlens arrays is decreased when both polarizations are considered. Corresponding optical crosstalk values are given with the reference values in Table 1.

Optical crosstalk is one of the two components of spatial crosstalk in IR-FPA pixels and the other one is the electrical crosstalk [1]. In the reference refractive microlens study, the spatial crosstalks for the reference system and refractive microlens system were found to be 2.82% and 2.9%, respectively. Compared with their optical crosstalk performances, the resulting spatial crosstalk is much closer and this was explained as a potential reduction in the spatial crosstalk due to much narrowed Airy disk in refractive microlenses. The reference system had a normal halfwidth of 9 μm, which was reduced to 3μm (corresponding to roughly 9-fold narrowing) with refractive microlens arrays. The normal halfwidths of our designs are shorter than 1.0, 1.2, 1.7 and 2 μm for the focal length parameters of 10, 20, 30 and 40 μm, respectively, (for the reference system having a 7.74 μm normal width ($\lambda_0 F_{\#}$)). A substantial narrowing is thus achieved here with the metasurface-based microlens arrays (narrowing roughly by 38-folds). This substantial narrowing should also lead to further improvement of the spatial crosstalk in IR-FPAs with metasurface-based microlenses already allowing for much weaker optical crosstalk.

#246090 Received 17 Jul 2015; revised 27 Aug 2015; accepted 30 Aug 2015; published 5 Oct 2015
© 2015 OSA

Table 1. Percentages of optical energy in the central and neighbor pixels.

IR-FPAs	Halfwidth (μm)	Optical crosstalk (%)
Reference	7.7	2.2
Refractive microlens	2.6	2.6
f = 10 μm metasurface	1.0	0.8
f = 20 μm metasurface	1.2	1.0
f = 30 μm metasurface	1.7	2.0
f = 40 μm metasurface	2.0	1.4
f = 50 μm metasurface	2.2	1.9

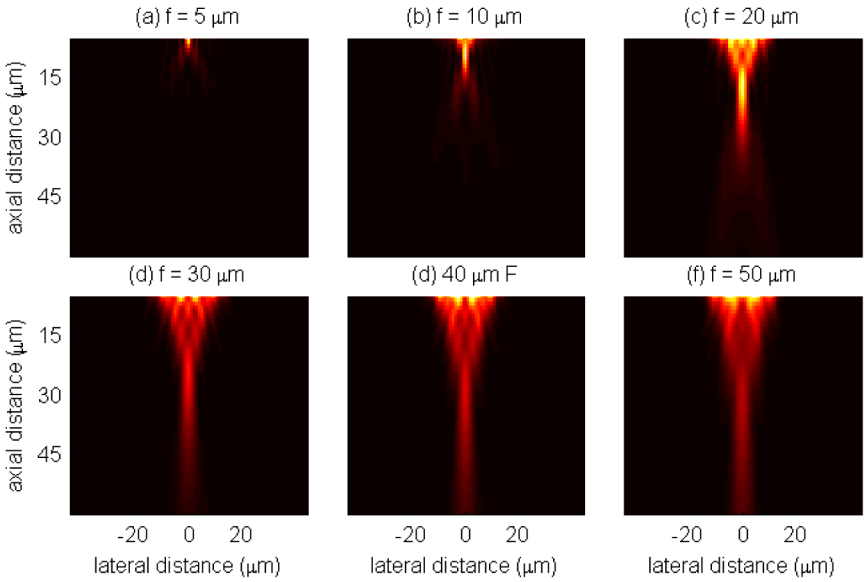

Fig. 4. Intensity distributions of the cross-polarized field obtained by illuminating the central unit cell of the proposed metasurface-based FPAs.

4. Conclusion

In summary, we have proposed and demonstrated metasurface-based microlens focal plane array designs that consist of asymmetrically-tailored V-shaped optical antennas, and discussed their functionality in narrowing the incident light beam width for optical crosstalk suppression. This work is the first account of optical crosstalk suppression using optical antennas. The concept of introducing abrupt phase shifts was applied in realizing these FPAs with metasurfaces. The expected behavior of microlens arrays was also confirmed with FDTD simulations and performance of the resulting structure was compared in terms of per-pixel intensity distributions and normal halfwidth of these distributions. Metasurface-based microlens arrays with subwavelength control of phase shift response allows for strong optical crosstalk suppression in mid-wave IR-FPAs enabling high spatial resolution and small pixel size.

#246090 Received 17 Jul 2015; revised 27 Aug 2015; accepted 30 Aug 2015; published 5 Oct 2015
© 2015 OSA